THE JOURNAL OF PHYSICAL CHEMISTRY C

Article

Cite This: J. Phys. Chem. C 2019, 123, 5321−5325

pubs.acs.org/JPCC

Effect of Grain Boundaries on Charge Transport in Methylammonium Lead Iodide Perovskite Thin Films

Hamidreza Khassaf,* Srinivas K. Yadavalli, Yuanyuan Zhou, Nitin P. Padture, and Angus I. Kingon

School of Engineering, Brown University, Providence, Rhode Island 02912, United States

ABSTRACT: Methylammonium lead iodide ($MAPbI_3$) has attracted great interest as an organic−inorganic hybrid perovskite for photovoltaic applications. Vacancy-mediated ion migration is one of the dominant carrier transport mechanisms in $MAPbI_3$. Our previous work clarified the nature of migrating species and their moderating effect on electronic transport. However, to develop strategies to mitigate ion migration and its impact thereof, it is important to know whether the migration is homogeneous or controlled by microstructural features, such as grain boundaries. In this work, we implement temperature-dependent pulsed voltage−current measurements of $MAPbI_3$ thin films with different grain sizes under dark conditions and distinguish the electromigration of iodine vacancies and methylammonium vacancies. Upon increasing the grain size, the total accumulated charge decreases, whereas the activation energies increase. This is consistent with the high grain boundary density in small-grained films responsible for facilitating charge transport. These results suggest that one viable strategy to decrease ion migration would be to engineer the grain boundaries of $MAPbI_3$.

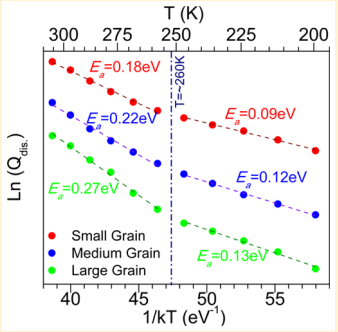

INTRODUCTION

There has been a surge of interest in organic−inorganic halide perovskites (OIHPs) for use in perovskite solar cells (PSCs) and other optoelectronic devices.[1−4] This is because OIHPs have been shown to have exceptional electrical and optical properties, such as low trap-density, strong optical absorption,[5] and long carrier-diffusion lengths. PSCs, in particular, offer the promise of being low-cost, and now the record efficiency of PSCs has reached 23.7%, rivaling that of silicon solar cells.[6] However, some of the fundamental properties of OIHPs are still not fully understood. Among them are ferroelectricity;[7] dielectric properties and the hysteretic nature of charge transport;[7,8] degradation resulting from field- and light-induced phase segregations;[8,9] and also the effect of the nature of point defects on their electrical behavior.[10] In particular, ion migration has attracted attention due to its correlation with the observed hysteresis behavior in OIHPs,[11,12] the impact on electronic charge transport,[13] and the likely impact on device degradation and failure. Several studies have been performed on electric field (E)-induced, room temperature migration of point defects in $CH_3NH_3PbI_3$ ($MAPbI_3$) OIHP, suggesting ion migration as the dominant phenomenon.[14,15] In this context, we previously reported our work that clarified the debate on ion migration[11,16−21] and clearly showed the contribution of vacancy-mediated migration of both MA^+ and I^- ions, each with distinct activation energy.[13] That work utilized temperature- and field-dependent pulsed $I−V$ measurements to separate ionic and electronic contributions under dark conditions, showing that the effects are related to the $MAPbI_3$ material itself, and are not ascribable to a particular device structure.[20] The work showed that the accumulation of ions at the ion-blocking electrodes modifies the electronic charge transport across the interface, moderating the $I−V$ behavior.

The previous work left open the question as to whether microstructure features can control the ion migration rates. For example, grain-boundary diffusion rates of ions are typically different from those of the bulk, both higher or lower. Reduced grain-boundary diffusion rates can act to block ion diffusion if the boundaries are transverse to the field direction and increased boundary diffusion can allow boundaries to act as conduits for transport, particularly if parallel to the field direction.[22] Shao et al.[15] used conductive atomic force microscopy (AFM) to examine ion transport locally in polycrystalline $MAPbI_3$ thin films in different regions of the bulk and at the grain boundaries. They measured larger hysteresis at grain boundaries compared to the bulk, leading them to infer faster ion migration at the grain boundaries. In this context, we set out to measure directly the activation energies of $MAPbI_3$ films with different grain sizes, controlling other conditions, to determine the effect of grain boundaries on ion migration. We adopted the same temperature-dependent pulsed $I−V$ strategy as in our previous work to ensure that electronic transport does not obscure ionic charge contributions.

EXPERIMENTAL PROCEDURE

We fabricated devices with a typical metal−semiconductor−metal (M−S−M) configuration, consisting of $MAPI_3$ films with three different average grain sizes asymmetrically

Received: February 3, 2019
Published: February 11, 2019

DOI: 10.1021/acs.jpcc.9b00538
J. Phys. Chem. C 2019, 123, 5321−5325

sandwiched between fluorine-doped tin oxide (FTO) and Au as bottom and top electrodes, respectively (Figure 1).

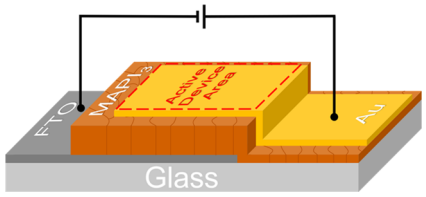

Figure 1. Schematic illustration of the M−S−M device with FTO−$MAPbI_3$−Au configuration. The dashed rectangle indicates the active device area.

The work function of both electrodes in such a device is close to 5 eV.[23] We cut 15 × 15 mm^2 squares of FTO substrates (Hartford Glass) with a sheet resistance of 8 Ω/sq, which were then etched using zinc dust and dilute aqueous hydrochloric acid. As for the cleaning process, substrates were washed using soap and deionized water and subsequently with absolute ethanol. In the final stage, they underwent ozone treatment for approximately 30 min before film deposition. A solution-based process was used to deposit $MAPI_3$ films onto FTO substrates as follows.[25] A 40 wt % $MAPbI_3$ solution was prepared by dissolving PbI_2 (99.9995%, Sigma-Aldrich) and MAI (Dyesol, Australia) in a stoichiometric (1:1) ratio in *N*,*N*-dimethylformamide (DMF) solvent. The precursor solution was spin-coated on a cleaned FTO substrate at 2000 rpm for 30 s while toluene was dripped at the 10th second of spinning. The baseline thin films were then annealed at 100 °C, while being exposed to DMF solvent vapor, for various durations (up to 10 min) to achieve various grain sizes using a setup similar to that used by Xiao et al.[24] Briefly, the substrate with the as-deposited thin film was placed on a preheated hotplate, then a 10 μL drop of the solvent was placed 2 cm from the closest edge of the substrate on a glass slide. The substrate and the glass slide with the solvent drop were covered immediately with an inverted glass Petri dish. The final $MAPbI_3$ films had thicknesses of ∼300 nm, as determined by cross-sectional scanning electron microscopy (SEM) of the films. To prevent degradation in the process of making the OIHP, all steps of film preparation were performed inside an N_2-filled glovebox. The $MAPbI_3$ thin films were characterized by X-ray diffraction (XRD; D8 Discover, Bruker, Germany) using Cu Kα radiation. The microstructures of the thin films were characterized using SEM (Leo, Zeiss, Germany). To estimate the average grain sizes, we used the intercept technique where the average grain sizes were calculated based on the intercepting grains in several random straight lines that were drawn through the SEM image. Au contacts of ∼120 nm thickness were evaporated and deposited on top of the films with a rate of ∼0.5 A/s and under a pressure of 10^{-6} Torr using a shadow mask. The active area (indicated by the dashed rectangle in Figure 1) is 5 mm^2.

RESULTS AND DISCUSSION

Figure 2a−c show the XRD patterns of the $MAPbI_3$ films with three different average grain sizes, confirming the presence of a pure tetragonal phase (space group *I*4/*mcm*). Figure 2d−f show the top-view SEM images of the corresponding $MAPbI_3$ thin films. The SEM images show smooth, dense, and uniform surfaces throughout the active device area in all three films. The average grain sizes of small-, medium-, and large-grained

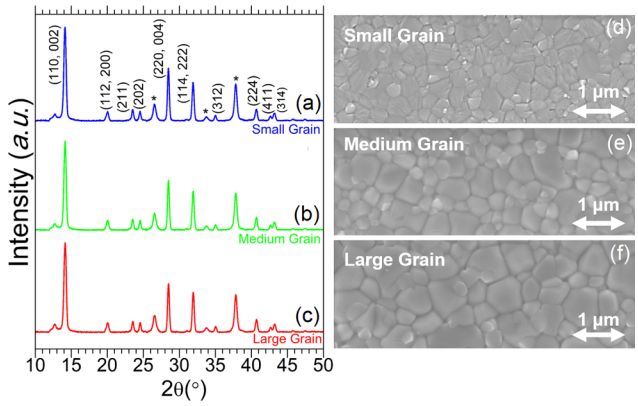

Figure 2. XRD patterns of representative $MAPbI_3$ thin films with different microstructures: (a) small-grained (∼413 nm), (b) medium-grained (∼535 nm), and (c) coarse-grained (∼628 nm). (*Indicates reflections from the underlying FTO.) Top-view SEM micrographs of representative $MAPbI_3$ thin films with different microstructures: (d) small-grained (∼413 nm), (e) medium-grained (∼535 nm), and (f) coarse-grained (∼628 nm).

thin films are estimated to be ∼413, ∼535, and ∼628 nm, respectively. Also, in all three sample types, the growth is columnar due to the large grain size to thickness ratio of the films (∼1.38, ∼1.78, and ∼2.1, respectively). This is important, as it implies that the grain boundaries are primarily oriented in the direction of the field.[24,25]

To perform temperature-dependent measurements, the M−S−M device was quickly placed (to minimize exposure to air) in a cryostat chamber (VPF-100, Janis), where it was kept under vacuum (pressure of ∼10^{-3} Torr) throughout the measurements. A temperature controller (335, Lakeshore) was used inside the cryostat to stabilize the device at the desired temperature. Electrical measurements were performed using a sourcemeter (2635A, Keithley). For consistency, the Au top electrode was always connected to the "high" and the FTO bottom electrode was always connected to the "low" leads of the sourcemeter. Figure 3 shows the grain size dependence of the cyclic *I*−*V* responses starting from 0 V.

The hysteresis in the *I*−*V* curve for $MAPbI_3$ shows strong dependence on the average grain size, confirming the results

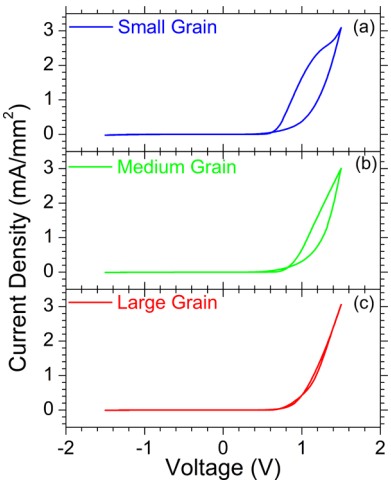

Figure 3. *I*−*V* curves from $MAPI_3$ thin films of different microstructures: (a) small-grained (∼413 nm), (b) medium-grained (∼535 nm), and (c) coarse-grained (∼628 nm).

DOI: 10.1021/acs.jpcc.9b00538
J. Phys. Chem. C 2019, 123, 5321−5325

reported by Shao.[7] It is clear that as the average grain size decreases, the current hysteresis increases. Since greater current hysteresis indicates faster ion migration during the current scanning process, these results indicate that grain boundaries affect ion migration.[15] Here, one can expect strong temperature dependency in the current-leakage characteristics. Thus, temperature-dependent pulsed voltage−current measurements, that are traditionally used in the study of the relaxation phenomenon in dielectrics,[26] can be particularly informative as it allows us to distinguish electronic, ionic, and dielectric displacement contributions. In this method, continuous application of voltage results in an immediate rise of current. The magnitude of this current reaches a stable value after some time (typically ∼10 s). At this point, upon removal of the applied voltage, there is a discharge current of opposite sign relative to the initial current. This is due to the fact that the applied voltage causes charge accumulation at the interface which will dissipate upon removal of the field. This accumulated charge (Q_{dis}) at the interface can be measured by integrating the discharge current over time.

Figure 4a shows the plot of the temperature-dependent discharge current after continuous application of 1.25 V for a

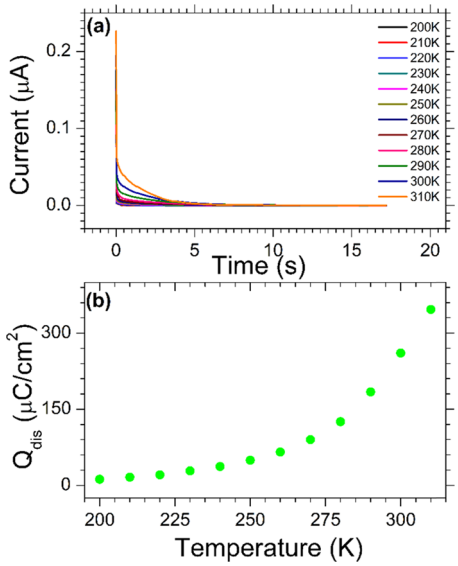

Figure 4. (a) Temperature-dependent discharge currents as a function of time after V = 1.25 V is applied continuously. (b) Corresponding accumulated charge (Q_{dis}) as a function of temperature.

representative device. As is evident, transient discharge currents show very strong temperature dependence in the range of 200−310 K upon removal of voltage. Figure 4b presents the corresponding Q_{dis} as a function of temperature. Here, the Q_{dis} originates from capacitive effects predominantly due to ion accumulation rather than dielectric polarization—if the latter was dominant, then Q_{dis} would have correlated with temperature-dependent permittivity that shows a sharp maximum associated with the phase transition at ∼160 K.[27] A more detailed explanation of this distinction can be found elsewhere.[13] The observed exponentially increasing Q_{dis} with temperature indicates a thermally activated mechanism for the accumulation of charge. Therefore, one can use the Arrhenius equation to express and quantify the phenomenon as follows

$$Q = Q_0 \exp\left(\frac{E_a}{kT}\right) \quad (1)$$

where Q is the accumulated charge, Q_0 is the pre-exponential factor, k is the Boltzmann constant, T is the temperature, and E_a is the activation energy for the migration of charged species. The results are plotted in Figure 5 plots for the three devices with different average grain sizes.

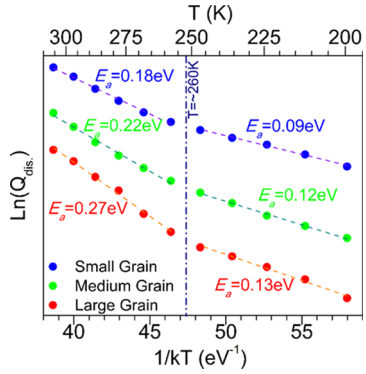

Figure 5. Arrhenius representation of Q_{dis} obtained from three devices with different average grain sizes upon removal of a continuous voltage of V = 1.25 V.

Similar to what was observed and discussed in our previous work,[13] the plotted ln(Q_{dis}) vs $1/kT$ shows two distinct slopes in all three devices, with a "knee" in all the data at ∼260 K. This implies the existence of two distinct and distinguishable thermally activated processes in all the devices. The lower temperature activation energies are 0.09, 0.12, and 0.13 for small-, medium-, and large-grained $MAPbI_3$ thin films, respectively. At temperatures above 260 K, the activation energies are 0.18, 0.22, and 0.27 eV for small-, medium-, and large-grained $MAPbI_3$ thin films, respectively. The presence of these two thermally activated processes with considerably different activation energies suggests the migration and accumulation of two different species, which we previously attributed for vacancy-mediated migration of I^- and MA^+ for lower and higher values of E_a, respectively.[13] More interestingly, as the grain size increases, the magnitude of E_a in both cases increases. This is in line with the results of a recent study that suggests that the concentration of the mobile MA^+ ions near grain boundaries is one order of magnitude higher than the bulk,[28] which implies that grain boundaries may have a significant effect on the activation energy of MA^+ ions. We note that these measurements were repeated on several meticulously prepared samples, where there were three to four different regions in each sample that were electroded for pulse-discharge measurements. The margin of error was calculated to be less than 0.45% for both types of calculated activation energies implying a high degree of reproducibility.

We should mention that as we have shown in our recent study,[12] in an OIHP, depending on the level of activity of the present ionic species, there could be three observed dynamic behaviors in electronic charge transport. It could vary from an Ohmic behavior with no $I-V$ hysteresis, to an ionic migration-dominated behavior, and finally to an ionic accumulation-dominated behavior before it breaks down. Based on our findings in this work, we have chosen a continuous voltage of V = 1.25 V before removal to ensure that the device is in its ionic accumulation-dominated response region. This could be one of

DOI: 10.1021/acs.jpcc.9b00538
J. Phys. Chem. C 2019, 123, 5321−5325

the determining factors to obtain highly reproducible results as the strong field and sufficient time would facilitate exhaustion in accumulation of the ionic species present at the interface and allow for capturing the full extent of their effect during the pulse-discharge measurements. Moreover, it is important to note that although we have shown definitively that the activation energies correlate with the grain size, and the results are highly reproducible for a given process method, the grain sizes are not the only parameters impacting the activation energies. Other experimentally measured activation energies for material systems similar to ours are within a wide range of 0.1−0.6 eV.[16,17,21] And even within our own lab, depending on the process method, the activation energy for the higher temperature mechanism, i.e. for MA^+ ion diffusion, has been seen to vary even after accounting for grain size. Based upon observations from multiple process routes, our indirect conclusion is that the process method strongly impacts the concentration of A-site vacancies, particularly at grain boundaries and interfaces. This is consistent with the known facile nature of methylammonium and methylammonium iodide evaporation and the high concentration of A-site and anion vacancies that can be accommodated in the perovskite structure.

It is also noteworthy that a photoluminescence microscopic study has revealed the presence of special subgrain boundaries in halide perovskites that are not observed using conventional methods such as AFM and SEM.[29] Therefore, it is important that the reader keeps in mind that what we call grain size in this paper is in fact the apparent grain size and does not account for these subgrain boundaries. In the future, careful TEM analyses may be adopted for deep understanding of the nature of grain bouandaries.[30] Besides, the processing temperature is kept as low as ∼100 °C for durations less than 10 min for all devices. Therefore, it is reasonable to assume that it is unlikely to have different surface energies in various samples.

CONCLUSIONS

In summary, we characterized the ion migration behavior of OIHP $MAPbI_3$ thin films with various grain sizes and under dark conditions. We adopted a pulsed voltage−current measurement scheme that decouples ion migration and accumulation from electronic transport with the aim of studying the effect of grain size on the charge transport phenomenon. By performing capacitive discharge measurements at various temperatures, we calculated the E_as for devices with different structural characteristics. We show that two distinct thermally activated processes exhibit different E_a values in each device, and we established a clear trend in which as the grain size increases, the magnitudes of E_a increase for both types of migrating species. We demonstrate that while the grain boundaries are not the only parameters impacting the activation energies, it is abundantly clear that activation energies correlate with the grain size. These results provide insights into previous studies on the effect of high-energy regions in OIHPs and present a confirmation that grain boundaries as high-energy regions through the bulk and at the interface have a high impact on ion migration and consequently the charge transport phenomenon in OIHPs. These results, therefore, suggest that a practical strategy to decrease ion migration would be to tune and engineer the grain boundaries of OIHPs.

AUTHOR INFORMATION

Corresponding Author

*E-mail: hamidreza_khassaf@brown.edu.

ORCID

Hamidreza Khassaf: 0000-0002-9869-0745
Nitin P. Padture: 0000-0001-6622-8559
Angus I. Kingon: 0000-0002-0767-2892

Notes

The authors declare no competing financial interest.

ACKNOWLEDGMENTS

This research was supported by the National Science Foundation (Grant No. OIA-1538893).

REFERENCES

(1) Stranks, S. D.; Snaith, H. J. Metal-Halide Perovskites for Photovoltaic and Light-Emitting Devices. *Nat. Nanotechnol.* **2015**, *10*, 391.

(2) Zhang, W.; Eperon, G. E.; Snaith, H. J. Metal Halide Perovskites for Energy Applications. *Nat. Energy* **2016**, *1*, 16048.

(3) Egger, D. A.; Bera, A.; Cahen, D.; Hodes, G.; Kirchartz, T.; Kronik, L.; Lovrincic, R.; Rappe, A. M.; Reichman, D. R.; Yaffe, O. What Remains Unexplained About the Properties of Halide Perovskites? *Adv. Mater.* **2018**, *30*, No. 1800691.

(4) Dunlap-Shohl, W. A.; Zhou, Y.; Padture, N. P.; Mitzi, D. B. Synthetic Approaches for Halide Perovskite Thin Films *Chem. Rev.* 2018, .

(5) De Wolf, S.; Holovsky, J.; Moon, S.-J.; Löper, P.; Niesen, B.; Ledinsky, M.; Haug, F.-J.; Yum, J.-H.; Ballif, C. Organometallic Halide Perovskites: Sharp Optical Absorption Edge and Its Relation to Photovoltaic Performance. *J. Phys. Chem. Lett.* **2014**, *5*, 1035−1039.

(6) Green, M. A.; Hishikawa, Y.; Dunlop, E. D.; Levi, D. H.; Hohl-Ebinger, J.; Yoshita, M.; Ho-Baillie, A. W. Solar Cell Efficiency Tables (Version 53). *Prog. Photovoltaics* **2019**, *27*, 3−12.

(7) Kutes, Y.; Ye, L.; Zhou, Y.; Pang, S.; Huey, B. D.; Padture, N. P. Direct Observation of Ferroelectric Domains in Solution-Processed $CH_3NH_3PbI_3$ Perovskite Thin Films. *J. Phys. Chem. Lett.* **2014**, *5*, 3335−3339.

(8) Hoke, E. T.; Slotcavage, D. J.; Dohner, E. R.; Bowring, A. R.; Karunadasa, H. I.; McGehee, M. D. Reversible Photo-Induced Trap Formation in Mixed-Halide Hybrid Perovskites for Photovoltaics. *Chem. Sci.* **2015**, *6*, 613−617.

(9) Zhang, W.; Burlakov, V. M.; Graham, D. J.; Leijtens, T.; Osherov, A.; Bulović, V.; Snaith, H. J.; Ginger, D. S.; Stranks, S. D. Photo-Induced Halide Redistribution in Organic−Inorganic Perovskite Films. *Nat. Commun.* **2016**, *7*, No. 11683.

(10) Brenner, T. M.; Egger, D. A.; Kronik, L.; Hodes, G.; Cahen, D. Hybrid Organic—Inorganic Perovskites: Low-Cost Semiconductors with Intriguing Charge-Transport Properties. *Nat. Rev. Mater.* **2016**, *1*, 15007.

(11) Snaith, H. J.; Abate, A.; Ball, J. M.; Eperon, G. E.; Leijtens, T.; Noel, N. K.; Stranks, S. D.; Wang, J. T.-W.; Wojciechowski, K.; Zhang, W. Anomalous Hysteresis in Perovskite Solar Cells. *J. Phys. Chem. Lett.* **2014**, *5*, 1511−1515.

(12) Khassaf, H.; Yadavalli, S. K.; Game, O. S.; Zhou, Y.; Padture, N. P.; Kingon, A. I. Comprehensive Elucidation of Ion Transport and Its Relation to Hysteresis in Methylammonium Lead Iodide Perovskite Thin Films *J. Phys. Chem. C* 2019, .

(13) Game, O. S.; Buchsbaum, G. J.; Zhou, Y.; Padture, N. P.; Kingon, A. I. Ions Matter: Description of the Anomalous Electronic Behavior in Methylammonium Lead Halide Perovskite Devices. *Adv. Funct. Mater.* **2017**, *27*, No. 1606584.

(14) Yuan, Y.; Huang, J. Ion Migration in Organometal Trihalide Perovskite and Its Impact on Photovoltaic Efficiency and Stability. *Acc. Chem. Res.* **2016**, *49*, 286−293.

DOI: 10.1021/acs.jpcc.9b00538
J. Phys. Chem. C 2019, 123, 5321−5325

(15) Shao, Y.; Fang, Y.; Li, T.; Wang, Q.; Dong, Q.; Deng, Y.; Yuan, Y.; Wei, H.; Wang, M.; et al. Grain Boundary Dominated Ion Migration in Polycrystalline Organic−Inorganic Halide Perovskite Films. *Energy Environ. Sci.* **2016**, *9*, 1752−1759.
(16) Yuan, Y.; Chae, J.; Shao, Y.; Wang, Q.; Xiao, Z.; Centrone, A.; Huang, J. Photovoltaic Switching Mechanism in Lateral Structure Hybrid Perovskite Solar Cells. *Adv. Energy Mater.* **2015**, *5*, No. 1500615.
(17) Azpiroz, J. M.; Mosconi, E.; Bisquert, J.; De Angelis, F. Defect Migration in Methylammonium Lead Iodide and Its Role in Perovskite Solar Cell Operation. *Energy Environ. Sci.* **2015**, *8*, 2118−2127.
(18) Li, C.; Tscheuschner, S.; Paulus, F.; Hopkinson, P. E.; Kießling, J.; Köhler, A.; Vaynzof, Y.; Huettner, S. Iodine Migration and Its Effect on Hysteresis in Perovskite Solar Cells. *Adv. Mater.* **2016**, *28*, 2446−2454.
(19) Meloni, S.; Moehl, T.; Tress, W.; Franckevičius, M.; Saliba, M.; Lee, Y. H.; Gao, P.; Nazeeruddin, M. K.; Zakeeruddin, S. M.; et al. Ionic Polarization-Induced Current−Voltage Hysteresis in $CH_3NH_3PbI_3$ Perovskite Solar Cells. *Nat. Commun.* **2016**, *7*, No. 10334.
(20) Richardson, G.; O'Kane, S. E.; Niemann, R. G.; Peltola, T. A.; Foster, J. M.; Cameron, P. J.; Walker, A. B. Can Slow-Moving Ions Explain Hysteresis in the Current−Voltage Curves of Perovskite Solar Cells? *Energy Environ. Sci.* **2016**, *9*, 1476−1485.
(21) Eames, C.; Frost, J. M.; Barnes, P. R.; O'regan, B. C.; Walsh, A.; Islam, M. S. Ionic Transport in Hybrid Lead Iodide Perovskite Solar Cells. *Nat. Commun.* **2015**, *6*, No. 7497.
(22) Adhyaksa, G. W.; Brittman, S.; Āboliņš, H.; Lof, A.; Li, X.; Keelor, J. D.; Luo, Y.; Duevski, T.; Heeren, R. M.; Ellis, S. R.; et al. Understanding Detrimental and Beneficial Grain Boundary Effects in Halide Perovskites. *Adv. Mater.* **2018**, *30*, No. 1804792.
(23) Helander, M. G.; Greiner, M.; Wang, Z.; Tang, W.; Lu, Z. Work Function of Fluorine Doped Tin Oxide. *J. Vac. Sci. Technol., A* **2011**, *29*, No. 011019.
(24) Xiao, Z.; Dong, Q.; Bi, C.; Shao, Y.; Yuan, Y.; Huang, J. Solvent Annealing of Perovskite-Induced Crystal Growth for Photovoltaic-Device Efficiency Enhancement. *Adv. Mater.* **2014**, *26*, 6503−6509.
(25) Jeon, N. J.; Noh, J. H.; Kim, Y. C.; Yang, W. S.; Ryu, S.; Seok, S. I. Solvent Engineering for High-Performance Inorganic−Organic Hybrid Perovskite Solar Cells. *Nat. Mater.* **2014**, *13*, 897.
(26) Lamhamdi, M.; Pons, P.; Zaghloul, U.; Boudou, L.; Coccetti, F.; Guastavino, J.; Segui, Y.; Papaioannou, G.; Plana, R. Voltage and Temperature Effect on Dielectric Charging for Rf-Mems Capacitive Switches Reliability Investigation. *Microelectron. Reliab.* **2008**, *48*, 1248−1252.
(27) Khassaf, H.; Khakpash, N.; Vijayan, S.; Aindow, M.; Alpay, S. Electrostatically Driven Dielectric Anomaly in Mesoscopic Ferroelectric−Paraelectric Bilayers. *Acta Mater.* **2016**, *105*, 68−74.
(28) Futscher, M. H.; Lee, J. M.; Wang, T.; Fakharuddin, A.; Schmidt-Mende, L.; Ehrler, B. Quantification of Ion Migration in $CH_3NH_3PbI_3$ Perovskite Solar Cells by Transient Capacitance Measurements. 2018, arXiv:1801.08519. arXiv.org e-Printarchive. https://arxiv.org/abs/1801.08519.
(29) Li, W.; Yadavalli, S. K.; Lizarazo-Ferro, D.; Chen, M.; Zhou, Y.; Padture, N. P.; Zia, R. Sub-Grain Special Boundaries in Halideperovskite Thin Films Restrict Carrier Diffusion. *ACS Energy Lett.* **2018**, 2669.
(30) Zhou, Y.; Sernlicht, H.; Padture, N. P. Transmission Electron Microscopy of Halide Perovskite Materials and Devices. *Joule* **2019**, DOI: 10.1016/j.joule.2018.12.011.

DOI: 10.1021/acs.jpcc.9b00538
J. Phys. Chem. C 2019, 123, 5321−5325